Journal of Magnetic Resonance 209 (2011) 101–107

Contents lists available at ScienceDirect

Journal of Magnetic Resonance

journal homepage: www.elsevier.com/locate/jmr

Communication

Selective detection of $^{13}CHD_2$ signals from a mixture of $^{13}CH_3/^{13}CH_2D/^{13}CHD_2$ methyl isotopomers in proteins

Xinli Liao [1], Vitali Tugarinov *

Department of Chemistry and Biochemistry, University of Maryland, College Park, MD 20742, United States

ARTICLE INFO

Article history:
Received 30 October 2010
Revised 29 December 2010
Available online 4 January 2011

Keywords:
Methyl isotopomer
Magic angle
Deuteration
J evolution

ABSTRACT

In NMR spectra of partially deuterated proteins methyl correlations are commonly observed as a combination of signals from $^{13}CH_3$, $^{13}CH_2D$ and $^{13}CHD_2$ isotopomers. In a number of NMR applications, methyl groups of the $^{13}CHD_2$ variety are targeted because of their AX-like character and concomitant simplification of the involved relaxation mechanisms. Although complete elimination of signals from $^{13}CH_2D$ methyl groups can be easily achieved in such applications, if the magnetization is not transferred through deuterium nuclei, efficient suppression of usually stronger $^{13}CH_3$ peaks is more problematic. A pair of simple pulse-scheme elements are presented that achieve almost complete suppression of $^{13}CH_3$ signals in the mixtures of $^{13}CH_3/^{13}CH_2D/^{13}CHD_2$ methyl isotopomers of small proteins at the expense of a moderate (~20-to-40%) reduction in intensities of the targeted $^{13}CHD_2$ groups. The approaches described are based purely on scalar coupling ($^1J_{CH}$) evolution properties of different ^{13}C and ^1H transitions within $^{13}CH_3$ spin-systems and are superior to magnetization transfer through deuterons with respect to sensitivity of the detected $^{13}CHD_2$ methyl signals.

1. Introduction

In protein samples either generated in D_2O media using protonated ^{13}C-labeled pyruvate as carbon source or obtained from ^{13}C-enriched glucose in a mixture of H_2O and D_2O solvents, methyl groups of $^{13}CH_3$, $^{13}CH_2D$, $^{13}CHD_2$ and $^{13}CD_3$ variety are produced [1–7]. Due to isotope shifts, the first three of this set of methyl isotopomers resonate at slightly different ^1H and ^{13}C frequencies degrading resolution in two-dimensional ^1H–^{13}C correlation spectra. In a variety of NMR applications, $^{13}CHD_2$ methyl isotopomers are targeted because ^{13}C relaxation in this isotopomer is amenable to straightforward interpretation [4,6,8–11]. Although complete elimination of signals from $^{13}CH_2D$ methyl groups can be easily achieved in applications that focus on isotopomers of $^{13}CHD_2$ variety, if no magnetization transfer through deuterons is involved, efficient suppression of usually stronger $^{13}CH_3$ peaks is significantly more problematic due to differential relaxation of the outer and inner components of the ^{13}C quartet in HSQC [12]-type magnetization transfer schemes [13–16] and the same parity of $^{13}CH_3$ and $^{13}CHD_2$ groups with respect to the number of ^1H spins.

Usually, purging elements are introduced into NMR pulse-schemes that dephase the magnetization terms of $^{13}CH_3$ spins-systems containing ^1H spins [4,7,9]. Even in small proteins such purging of $^{13}CH_3$ magnetization is only partially effective [7,9]. In larger molecules, where cross-correlated relaxation rates between ^{13}C–H dipoles within $^{13}CH_3$ methyl groups are faster, it achieves only marginal reduction in $^{13}CH_3$ signal intensities. Obviously, 'clean' $^{13}CHD_2$ detection can be achieved by the transfer of magnetization through ^2H spins. However, the associated sensitivity losses of $^{13}CHD_2$ signals ($\geqslant$50%) make this approach unattractive for applications that do not focus on ^2H relaxation measurements. To alleviate this problem, Ishima, Torchia and co-workers have introduced an optimized methyl labeling scheme that increases the content of $^{13}CHD_2$ isotopomers and reduces that of $^{13}CH_3$ methyls through the use of partially deuterated pyruvate and α-keto-butyrate for protein production [17].

We describe a pair of pulse-scheme elements that significantly improve the suppression of $^{13}CH_3$ signals in the mixtures of $^{13}CH_3/^{13}CH_2D/^{13}CHD_2$ methyl isotopomers of small (<~15 kDa) proteins at the expense of a moderate (~20-to-40%) reduction in intensities of the (targeted) $^{13}CHD_2$ methyls. Since the described approach is based purely on the properties of scalar coupling ($^1J_{CH}$) evolution of different transitions within the $^{13}CH_3$ spin-system, it is only slightly more tolerant to the effects of ^{13}C–^1H/^{13}C–^1H dipole–dipole cross-correlated relaxation, and is not effective in larger proteins. Nevertheless, 'chemical' labeling of $^{13}CHD_2$ methyl groups via the use of $^{13}CHD_2$-methyl-labeled

* Corresponding author. Address: Biomolecular Sci. Bldg./CBSO, Department of Chemistry and Biochemistry, University of Maryland, College Park, MD 20742, United States. Fax: +1 301 3140386.
E-mail address: vitali@umd.edu (V. Tugarinov).
[1] X.L. is on leave from the Department of Chemistry, Xiamen University, China.

1090-7807/$ - see front matter © 2011 Elsevier Inc. All rights reserved.
doi:10.1016/j.jmr.2010.12.014

biosynthetic precursors is much preferred for large proteins because the content of $^{13}CHD_2$ methyl labels is then close to 100% eliminating signal-to-noise/resolution losses associated with generation of isotopomers of other types [18–22].

2. Results and discussion

Improved suppression of $^{13}CH_3$ signals for selective detection of $^{13}CHD_2$ methyl isotopomers. Fig. 1 shows the HSQC pulse-scheme that can be used for selective detection of $^{13}CHD_2$ methyl isotopomers [4]. The pulse-scheme elements for ^{13}C $R_{1\rho}$, R_1 and CPMG measurements in $^{13}CHD_2$ groups can be inserted at the position indicated with the dashed rectangle. If 'purging' of $^{13}CH_3$ groups is employed [4,7,9], the dashed 90° ^1H pulse is applied in the element enclosed in the solid box in Fig. 1, with the delay 2ζ adjusted to $0.5/^1J_{CH}$ (4.0 ms for $^1J_{CH}$ = 125 Hz). Then, in the absence of dipole–dipole cross-correlated relaxation, the only $^{13}CH_3$ methyl magnetization terms that are created after the period 2ζ are of the $4C_xH_z^iH_z^j$ type, where i and j denote any two of the three ^1H spins (i, j = 1,2,3; $i \neq j$). These magnetization terms are purged by the dashed 90° ^1H pulse and subsequently de-phased by the gradient g5. In the presence of cross-correlated relaxation between the ^{13}C–^1H dipoles of the methyl group that leads to different relaxation rates of the outer and inner lines of the ^{13}C 3:1:1:3 quartet [13–16,23,24], the terms that are in-phase with respect to ^1H spins, C_x, will be created. These terms are immune to the ^1H purging pulse. Subsequently, after the delay 2Δ following the t_1 evolution period (Fig. 1), these terms will evolve into the magnetization of the type $8C_xH_z^iH_z^jH_z^k$ (i, j, k = 1,2,3; $i \neq j \neq k$) that will cross-relax with the terms $2C_xH_z^i$ (i = 1, 2, 3) which will in turn evolve into observable magnetization in the end of the pulse-scheme.

Significantly improved suppression of $^{13}CH_3$ signals is achieved when the purging 90° ^1H pulse (dashed in the solid box in Fig. 1) is not applied, and the delay 2ζ is adjusted to such a value that the evolution angle of the inner components of the methyl quartet, $2\pi J\zeta$, is equal to magic angle (54.7°; $J \equiv {}^1J_{CH}$ is the one-bond ^1H–^{13}C coupling in a methyl group). Fig. 2 shows the energy level diagram of a $^{13}CH_3$ spin-system where all the energy levels are numbered 1 through 16. It is straightforward to show that in the absence of relaxation, each of the outer transitions, ρ, of the methyl 3:1:1:3 quartet contributes to the final observable ^1H magnetization as follows [13,23–25]:

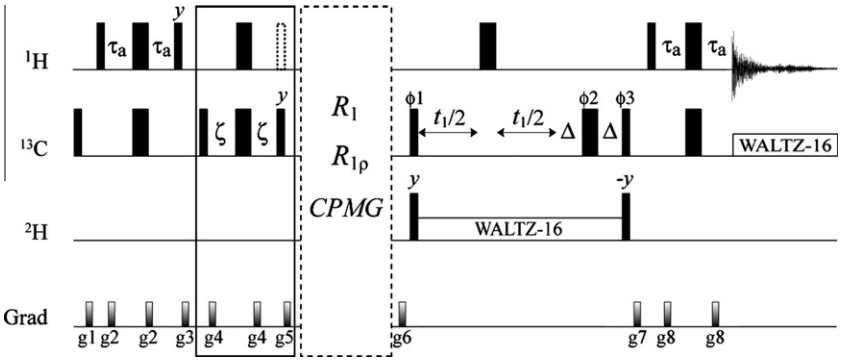

Fig. 1. The pulse-scheme for recording 2D single-quantum $^{13}CHD_2$ methyl ^1H–^{13}C correlation maps with suppression of signals from $^{13}CH_3$ and $^{13}CH_2D$ methyl isotopomers. All narrow (wide) rectangular pulses were applied with the flip angles of 90° (180°) along the x-axis unless indicated otherwise. The $^1H(^2H; ^{13}C)$ carriers are positioned at 0.8 (0.8; 22) ppm. All ^1H, ^2H and ^{13}C pulses are applied with maximum possible power. ^2H and ^{13}C WALTZ-16 decoupling [34] is applied with 0.9 and 2.5 kHz field strengths, respectively. Delays are: $\tau_a = \Delta$ = 2.0 ms ($0.25/^1J_{CH}$ for $^1J_{CH}$ = 125 Hz); ζ = 1.20 ms (see text for details). The ^1H 90° pulse shown with the dashed line is used only when purging of $^{13}CH_3$ methyl signals is employed. Then, the delay ζ is adjusted to 2.0 ms. The phase-cycle is: $\varphi1 = x,-x$; $\varphi2 = x,-x,y,-y$; $\varphi3 = y$; rec. = $x,-x,-x,x$. Quadrature detection in t_1 is achieved via the States-TPPI [35] incrementation of phase $\varphi3$. Durations and strengths of pulsed-field gradients in units of (ms;Gauss/cm) are: g1 = (1;15); g2 = (0.3;5); g3 = (1.2;12); g4 = (0.3;8); g5 = (1.0;15); g6 = (0.8;10); g7 = (0.6;12); g8 = (0.4;8).

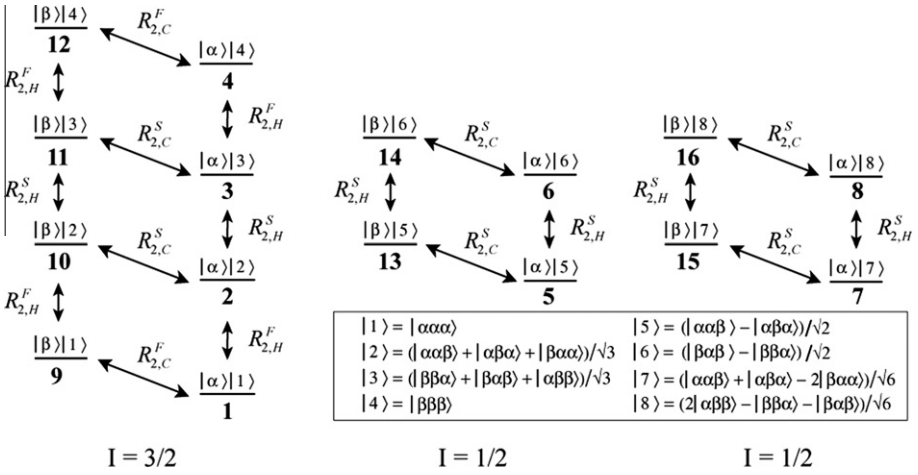

Fig. 2. Energy level diagram of a $^{13}CH_3$ spin system. Eigenfunctions corresponding to each of the three manifolds (one with the total spin number I = 3/2 and two with I = 1/2) are denoted by $|i\rangle|j\rangle$ where i and j refer to the ^{13}C and ^1H spin states, respectively. Vertical lines correspond to ^1H single-quantum (SQ) transitions; diagonal lines denote ^{13}C SQ transitions. $R_{2,H}^F$ and $R_{2,H}^S R_{2,C}^S$ denote the relaxation rates of slow and fast-relaxing ^1H transitions, respectively, while $R_{2,C}^F$ and $R_{2,C}^S$ are the respective relaxation rates of ^{13}C SQ transitions.

$$\rho_{1\leftrightarrow 9}\rho_{4\leftrightarrow 12} \rightarrow (9/2)\sin(6\pi J\zeta)\sin(6\pi J\Delta)M_H^{tr} \quad (1)$$

where M_H^{tr} is the transverse ^{1}H magnetization of ^{13}CH groups detected in the end of the pulse-scheme, and all the other delays are as shown in Fig. 1; while the contribution of each of the inner ^{13}C transitions is given by,

$$\rho_{2\leftrightarrow 10}\rho_{3\leftrightarrow 11}\rho_{6\leftrightarrow 14}\rho_{7\leftrightarrow 15}\rho_{8\leftrightarrow 16} \rightarrow (1/2)\sin(2\pi J\zeta)\sin(2\pi J\Delta)M_H^{tr} \quad (2)$$

For efficient elimination of $^{13}CH_3$ signals upon excitation of ^{1}H transitions later in the scheme, the J evolution should proceed until each of the outer transitions ($\rho_{1\leftrightarrow 9}\rho_{4\leftrightarrow 12}$) is opposite to the sum of the three inner transitions (one deriving from the manifold $I = 3/2$, e.g. $\rho_{2\leftrightarrow 10}$, and two from the manifolds $I = 1/2$, e.g. $\rho_{15\leftrightarrow 13}\rho_{7\leftrightarrow 15}$; see Fig. 2) thus leading to cancellation of the total $^{13}CH_3$ magnetization in the end of the pulse-scheme:

$$(9/2)\sin(6\pi J\zeta)\sin(6\pi J\Delta) = -3(1/2)\sin(2\pi J\zeta)\sin(6\pi J\Delta) \quad (3)$$

Solution of Eq. (3) for ζ with Δ fixed at $1/(4J)$ leads to the evolution angle $2\pi J\zeta$ equal to 0.9553 rad. (54.7356°), and the corresponding delay $2\zeta = 2.43$ ms for $J = 125$ Hz. The portion of the detected $^{13}CHD_2$ signal is then given by $\sin(2\pi J\zeta)$ that for $J = 125$ Hz and $\zeta = 2.43$ ms is 0.815 translating into the loss of $^{13}CHD_2$ intensity of 19% in the absence of relaxation.

It was realized much earlier that the use of magic angle pulses in DEPT [26] or analogously tuned delays in INEPT [27] pulse-schemes partially corrects for phase and intensity distortions [28] as well as eliminates the undesirable components of the signal that would interfere with ^{13}C relaxation time measurements in $^{13}CH_3$ groups [29]. Here, the 'magic angle evolution' is used to achieve a null in excitation of methyl ^{1}H magnetization in contrast to previous applications where the same evolution delay has been used to 'equilibrate' the contributions of different ^{13}C transitions to the observed methyl ^{1}H magnetization for the purpose of reliable ^{13}C R_2 relaxation rate measurements [14,30]. Fig. 3a shows a vector diagram illustrating the evolution of the outer ('3') and inner ('1') components of a $^{13}CH_3$ methyl during the de-phasing period 2ζ. After the first $^{13}C_x$ 90° pulse in the scheme of Fig. 1, the four magnetization components of $^{13}CH_3$ methyl groups are present in the 3:1:1:3 ratios. The outer lines of the quartet evolve to subtend an angle of 54.73° with respect to the y-axis after the time period 2ζ, while the two inner lines evolve to form an angle of $3 \times 54.73° = 164.2°$. Thus, after the period 2ζ, the projections of both components on the x-axis are equalized (Fig. 3a).

The treatment above is valid only in the absence of relaxation. The outer and inner lines of the ^{13}C quartet decay at very different rates [13–16,23]. Differential relaxation effects in $^{13}CH_3$ groups can be approximately accounted for assuming that each of the lines of the triplet relaxes exponentially leading to the following modulation for the resulting $^{13}CH_3$ signal,

$$S_{CH_3} = \left[3\sin(2\pi J\zeta)\exp(-R_{2,C}^S\tau) - 9\sin(6\pi J\zeta)\exp(-R_{2,C}^F\tau)\right]M_H^{tr} \quad (4)$$

where spin–spin relaxation of methyl protons during delays τ_a is neglected, $\tau = 2\zeta + 2\Delta + t_1 + T$, and T accounts for any additional delay(s) associated with relaxation measurements (Fig. 1); the relaxation rates $R_{2,C}^F$, $R_{2,C}^S$ of individual transitions are as shown in Fig. 2. In

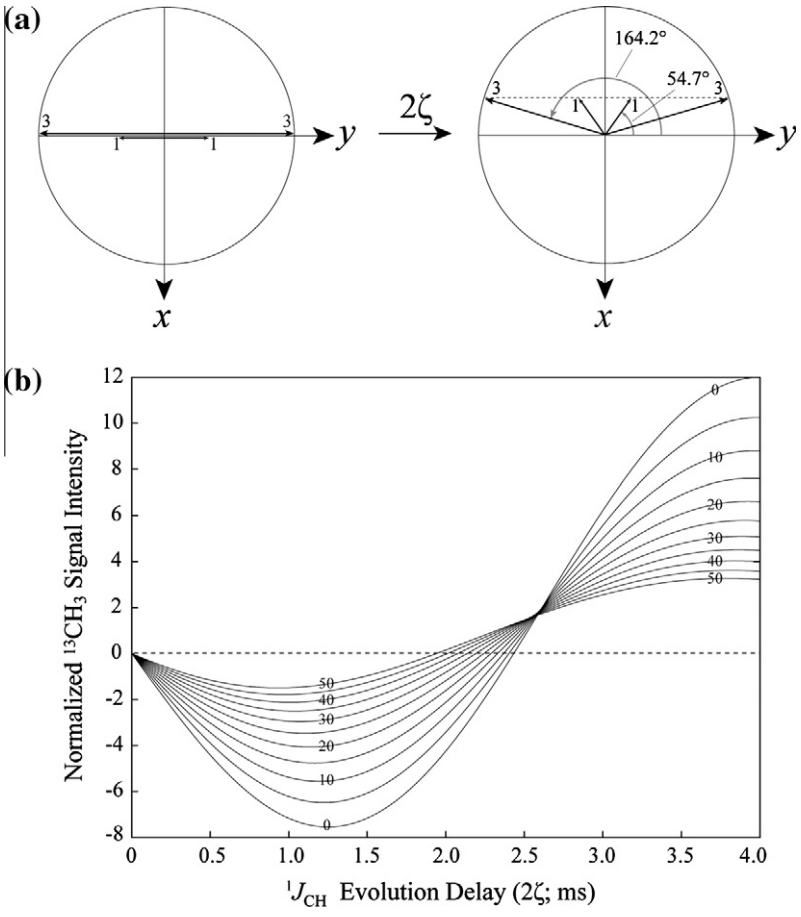

Fig. 3. (a) A vector diagram illustrating the evolution of the $^{13}CH_3$ methyl transverse magnetization components during the de-phasing period 2ζ. (b) A plot showing normalized signal intensity of $^{13}CH_3$ groups as a function of the J evolution delay 2ζ (ms) for $R_{2,C}^S$ rates in the range from 0 to 50 s^{-1}. The plots are calculated using Eq. (4) for $\tau = 2\zeta + 2\Delta$ ($t_1 = 0$; Fig. 1) and assuming $R_{2,C}^F/R_{2,C}^S = 5$. The horizontal dashed line is drawn at the null of the $^{13}CH_3$ signal.

the case of constant-time (CT) HSQC experiments [31] τ is equal to $2\zeta + T_C$, where T_C is the CT period. If only dipolar ^{13}C–^{1}H contributions are considered, $R^F_{2,C}/R^S_{2,C}$ [13,23]. However, if dipolar contributions due to external $^{1}H/^{2}H$ spins and methyl ^{13}C CSA relaxation are included, the ratio $R^F_{2,C}/R^S_{2,C}$ is calculated to amount to ~5. Fig. 3b shows normalized signal intensity of $^{13}CH_3$ groups (in units of M^{tr}_H) as a function of the J evolution delay 2ζ for $R^S_{2,C}$ rates in the range from 0 to 50 s^{-1}, calculated according to Eq. (4) for the first point in the F1 dimension ($t_1 = 0$; $\tau = 2\zeta + 2\Delta$; Fig. 1) and assuming $R^F_{2,C}/R^S_{2,C} = 5$. It is clear from Fig. 3b that a slight reduction of the delay 2ζ will lead to a better suppression of $^{13}CH_3$ signals in the presence of relaxation. Note that because of the differential relaxation of the four components of the quartet during the t_1 evolution period, each t_1 increment would correspond to a slightly different null of the $^{13}CH_3$ signal (Fig. 3b). Empirically, for the $t_{1,max}$ = 38 ms used here at both temperatures, the best suppression of $^{13}CH_3$ signals has been achieved on average when the delay 2ζ has been adjusted to a value 2%(5%) smaller in [3-$^{13}C_1$-pyruvate; 99% D_2O]-derived ubiquitin at 27 °C(5 °C) than the value of 2ζ in the absence of relaxation calculated above.

Improved suppression of $^{13}CH_3$ methyl signals has been achieved using the $^{13}CH_3$ 'magic angle evolution' delay in [3-$^{13}C_1$-pyruvate; 99% D_2O]-derived ubiquitin at 27(5) °C at the expense of on average 19(21)% reduction in signal intensity of $^{13}CHD_2$ methyls relative to the experiment with $^{13}CH_3$ methyl purging. The [3-$^{13}C_1$-pyruvate; 99% D_2O]-derived sample represents an especially unfavorable case with respect to $^{13}CH_3$ signal suppression because the initial average $^{13}CH_3/^{13}CHD_2$ intensity ratio observed in the ^{2}H-decoupled HSQC data set is 3.7(2.5) at 27 °C(5 °C). Fig. 4a–c show a selected region of the methyl ^{1}H–^{13}C single-quantum correlation maps recorded on the [3-$^{13}C_1$-pyruvate; 99% D_2O]-derived sample of ubiquitin (27 °C) using ^{1}H–^{13}C HSQC with ^{2}H decoupling (Fig. 4a), the pulse-scheme that purges $^{13}CH_3$ methyl signals (Fig. 4b), and the experiment of Fig. 1 with the delay 2ζ adjusted to 2.38 ms and no purging ^{1}H pulse applied (Fig. 4c). Comparisons of 1D slices drawn from the row of the 2D data sets shown with the dashed line in Fig. 4a–c at the ^{13}C chemical shift of $^{13}CHD_2$ isotopomers of Val^{17} γ2 and Leu^{50} δ2 methyls, are shown in Fig. 4d and e. The average $^{13}CH_3/^{13}CHD_2$ peak intensity ratios obtained using 'magic angle evolution' are 0.08 ± 0.06(0.15 ± 0.12) at 27 °C(5 °C) and compare well with the values of 0.61 ± 0.14(0.68 ± 0.18) at 27 °C(5 °C) obtained with purging of $^{13}CH_3$ magnetization. Of note, although complete suppression of $^{13}CH_3$ groups is achieved when the magnetization is filtered through ^{2}H nuclei, the average fraction of $^{13}CHD_2$ intensity observed is only 0.38(0.34) at 27 °C(5 °C).

Fig. 4f–h show a selected region of the methyl ^{1}H–^{13}C correlation maps recorded using the constant-time (CT) versions of the same set of pulse-schemes as in Fig. 4a–c recorded on the [U-^{13}C-glucose; 65% D_2O/35% H_2O]-derived ubiquitin. In this case,

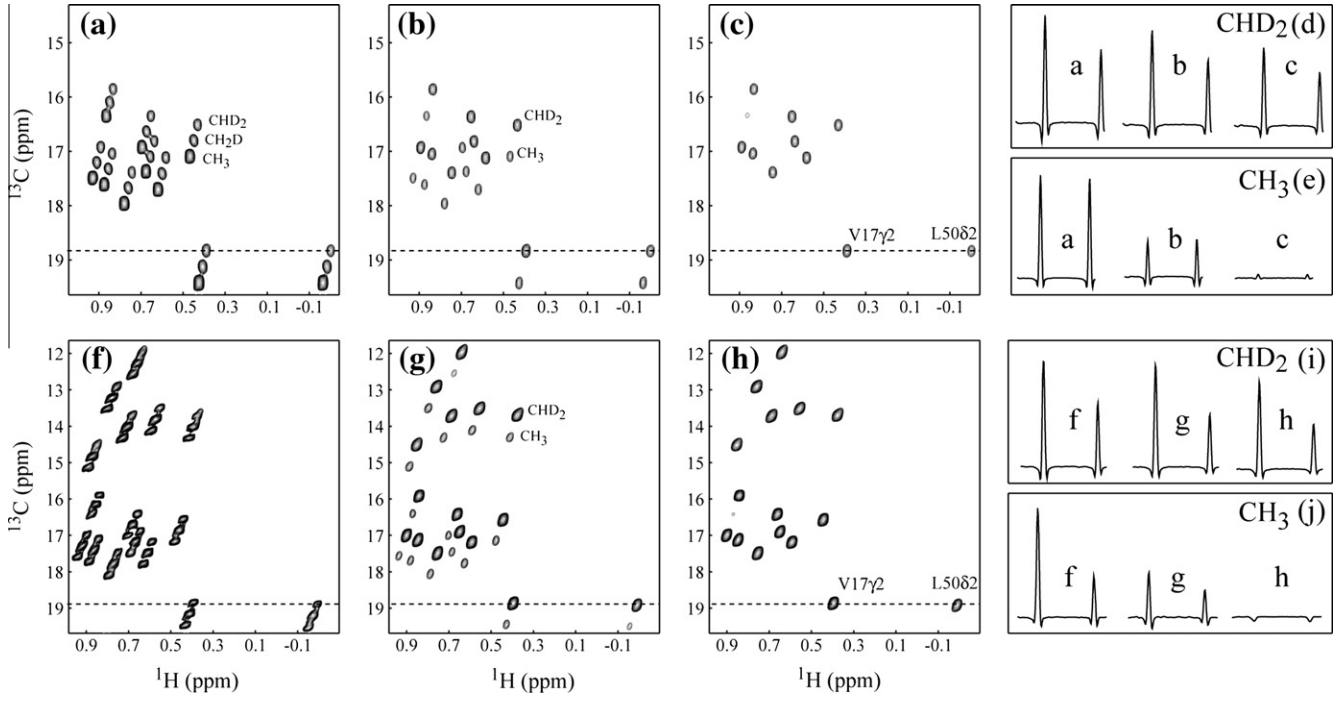

Fig. 4. (a–c) A selected region of the methyl ^{1}H–^{13}C single-quantum correlation maps recorded on the [3-$^{13}C_1$-pyruvate; 99% D_2O]-derived sample of ubiquitin using (a) ^{1}H–^{13}C HSQC pulse-scheme with ^{2}H decoupling; (b) the HSQC-based pulse-scheme that purges $^{13}CH_3$ methyl signals (with the dashed ^{1}H 90° pulse included and the delay 2ζ adjusted to 4 ms in the scheme of Fig. 1); (c) the pulse-scheme of Fig. 1 (without the dashed ^{1}H 90° pulse and the delay 2ζ adjusted to 2.4 ms). Exactly the same acquisition parameters have been used for all data sets (see below). The plots in a–c and f–h are drawn at the same contour levels. (d) A comparison of 1D slices drawn from the row of the 2D data sets shown with the dashed line in panels a–c at the ^{13}C chemical shift of $^{13}CHD_2$ isotopomers of Val^{17} γ2 and Leu^{50} δ2 methyl groups. (e) A comparison of the 1D slices drawn from the row of the 2D map corresponding to positions of $^{13}CH_3$ signals of Val^{17} γ2 and Leu^{50} δ2 in panels a–c. (f–h) A selected region of the methyl constant-time (CT) ^{1}H–^{13}C single-quantum correlation maps recorded on the [U-^{13}C-glucose; 65% D_2O/35% H_2O]-derived ubiquitin using (f) ^{1}H–^{13}C CT-HSQC; (g) CT-HSQC-based pulse-scheme that purges $^{13}CH_3$ signals; (h) the constant-time version of the pulse-scheme of Fig. 1. The CT period of $1/^{1}J_{CH}$ = 28 ms was used in all experiments. (i) A comparison of 1D slices drawn from the rows of the 2D data sets shown with dashed lines in (f–h) at the ^{13}C chemical shift of $^{13}CHD_2$ isotopomers of Val^{17} γ2 and Leu^{50} δ2 methyls. (j) A comparison of 1D slices drawn from the rows of the 2D map corresponding to positions of $^{13}CH_3$ signals of Val^{17} γ2 and Leu^{50} δ2 in panels (f–h). All experiments were performed on a 600 MHz Bruker Avance III spectrometer equipped with a room temperature triple-resonance probe. Both the [3-$^{13}C_1$-pyruvate; 99% D_2O]-derived and [U-^{13}C-glucose; 65% D_2O/35% H_2O]-derived samples of wild-type human ubiquitin were dissolved in a 20 mM 99.9% D_2O sodium phosphate buffer (uncorrected pH reading of 6.8) containing 0.03% NaN_3. The data sets comprised [512; 80] complex points in the [^{1}H; ^{13}C] dimensions with corresponding acquisition times of [64 ms; 38 ms]. A recovery delay of 2 s. was used (to account for longer ^{1}H T_1 relaxation times of $^{13}CHD_2$ methyl groups) along with 8 scans/FID giving rise to net acquisition times of ~50 min/experiment.

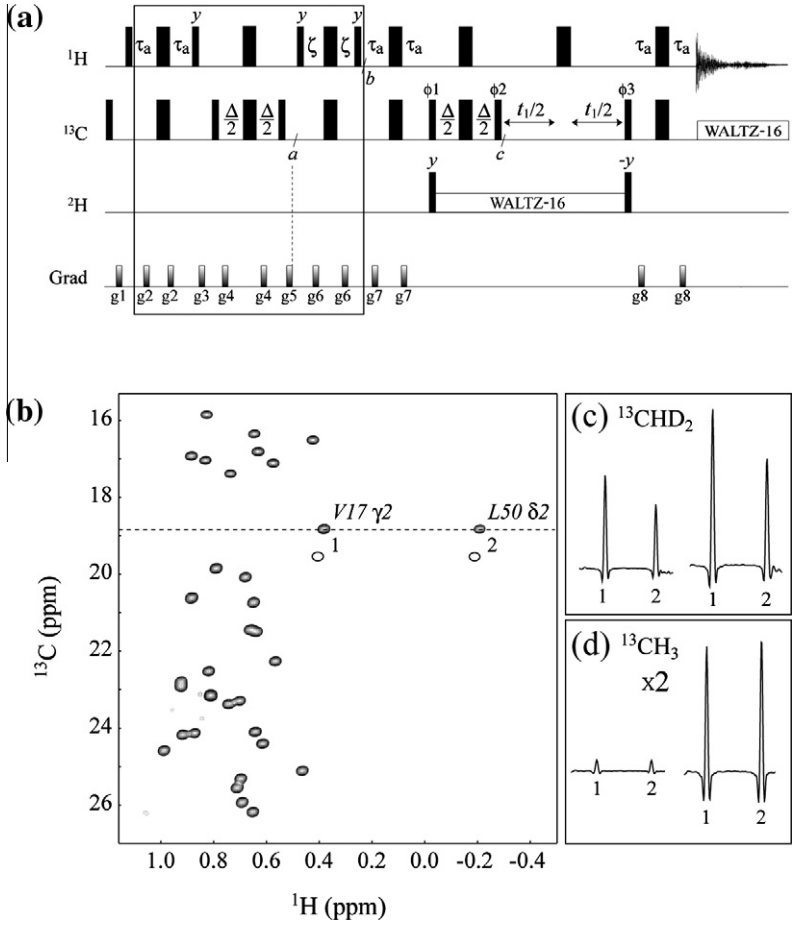

Fig. 5. (a) The pulse-scheme for recording 2D multiple-quantum $^{13}CHD_2$ methyl ^1H–^{13}C correlation maps with suppression of signals from $^{13}CH_3$ and $^{13}CH_2D$ methyl isotopomers. All the details of the pulse-scheme are the same as in Fig. 1. The phase-cycle is: $\varphi1 = x,-x$; $\varphi2 = 2(y), 2(-y)$; $\varphi3 = x$; rec. $= x,-x$. Quadrature in t_1 is achieved via the States-TPPI [35] incrementation of phase $\varphi3$. Durations and strengths of pulsed-field gradients in units of (ms;Gauss/cm) are: g1 = (1;15); g2 = (0.3;5); g3 = (1.2;15); g4 = (0.3;8); g5 = (0.8;10); g6 = (0.3;8); g7 = (0.5;10); g8 = (0.5;8). (b) The methyl region of the ^1H–^{13}C multiple-quantum correlation map recorded on the [3-$^{13}C_1$-pyruvate; 99% D_2O]-derived ubiquitin using the pulse-scheme shown in (a) The cross-peaks of Val^{17} $\gamma2$ (1) and Leu^{50} $\delta2$ (2) $^{13}CHD_2$ methyls are labeled, while the positions of $^{13}CH_3$ methyl peaks are below the contour levels of the plot and are shown with open ellipses. The data set is comprised of [512; 100] complex points in the [^1H; ^{13}C] dimensions with corresponding acquisition times of [64 ms; 48 ms]. A recovery delay of 2 s along with 8 scans/FID resulted in the net acquisition time of ~1 hr/experiment. (c) A comparison of the 1D slice drawn from the row of the 2D map shown with the dashed line (left) with the 1D slice from the 2D HSQC experiment recorded with purging of $^{13}CH_3$ signals and otherwise the same acquisition parameters (right). Both slices feature $^{13}CHD_2$ isotopomers of Val^{17} $\gamma2$ (1) and Leu^{50} $\delta2$ (2) methyls. (d) A comparison of the 1D slice drawn from the row of the 2D map corresponding to positions of $^{13}CH_3$ signals (shown with open ellipses in (b); left) with the corresponding 1D slice from the 2D HSQC experiment recorded with purging of $^{13}CH_3$ signals (right). Both slices feature $^{13}CH_3$ isotopomers of Val^{17} $\gamma2$ (1) and Leu^{50} $\delta2$ (2) methyls and are multiplied by a factor of 2 relative to the slices shown in panel c.

$^{13}CH_3/^{13}CHD_2$ intensity ratio observed in the ^2H-decoupled CT-HSQC data set (Fig. 4f) is only 1.3 on average (27 °C), and practically complete suppression of $^{13}CH_3$ methyls can be achieved using 'magic angle evolution' filtering. A comparison of 1D slices drawn from the rows of the 2D data sets shown with dashed lines in (f–h) at the ^{13}C chemical shift of $^{13}CHD_2$ isotopomers of Val^{17} $\gamma2$ and Leu^{50} $\delta2$ methyls are illustrated in Fig. 4i–j.

It is noteworthy that in any scheme that is based on scalar coupling ($^1J_{CH}$) evolution of different ^{13}C and ^1H transitions within $^{13}CH_3$ spin-systems, it is not possible to completely suppress all $^{13}CH_3$ signals because of (i) variations in the values of methyl $^1J_{CH}$ couplings, and (ii) variation in relaxation properties of different methyls. Moreover, the purely $^1J_{CH}$ evolution-based filtering described here is applicable and effective only in the limit when delays in the pulse-scheme (including the t_1 evolution period) are short compared to $(R^F_{2,C})^{-1}$. For example, although the 'magic angle'-based filtering is more effective than purging of $^{13}CH_3$ in terms of obtained $^{13}CH_3/^{13}CHD_2$ peak intensity ratios for any relaxation delay in the ^{13}C $R_{1\rho}$ relaxation measurements performed on [3-$^{13}C_1$-pyruvate; 99% D_2O]-derived ubiquitin at 27 °C, the efficiency of $^{13}CH_3$ suppression deteriorates fast: from the average $^{13}CH_3/^{13}CHD_2$ ratios of 0.08 ± 0.06 for initial relaxation delay to 0.43 ± 0.14 for the relaxation delay of 250 ms. Similarly, in an 82 kDa enzyme Malate Synthase G (isotropic correlation time $\tau_c \approx 45$ ns at 37 °C in D_2O) produced using [3-$^{13}C_1$]-pyruvate as carbon source in 99% D_2O, the $^{13}CH_3/^{13}CHD_2$ intensity ratio obtained after magic angle filtering is only slightly lower on average (0.74 ± 0.15) than that obtained when the $^{13}CH_3$ magnetization is purged (1.01 ± 0.21).

To estimate exactly how cross-correlated relaxation tolerant both $^{13}CH_3$ suppression schemes are, we have conducted simulations of the evolution of magnetization in $^{13}CH_3$ methyls in the presence of relaxation. Briefly, these simulations show that the 'magic angle evolution'-based scheme is somewhat more tolerant to ^{13}C–^1H/^{13}C-^1H dipole–dipole cross-correlations than the 'purging' scheme due to the fact that the *difference* in the fast- and slow-relaxing transitions of the $^{13}CH_3$ spin-system is sought for (Eqs. (3) and (4)). We have also attempted using the 'purging'

element in the end of the HSQC pulse-scheme (before the last INEPT magnetization transfer) where the refocusing of the purged-out multiple-quantum (MQ) ^{1}H terms is less likely as well as using composite 90° ^{1}H purging pulses. However, no significant improvement in $^{13}CH_3$ suppression was observed in either case indicating that the incompletely de-phased MQ ^{1}H magnetization is not the main determinant of the poor $^{13}CH_3$ suppression of the 'purging' scheme.

Other schemes for selective detection of $^{13}CHD_2$ methyl groups. Fig. 5a shows the multiple-quantum pulse-scheme developed for selective detection of $^{13}CHD_2$ isotopomers. Whereas in the scheme of Fig. 1 the elimination of $^{13}CH_3$ signals is achieved via searching for the null of carbon (^{13}C) transitions, here $^{13}CH_3$ signals are suppressed through obtaining the null of all proton (^{1}H) transitions in a $^{13}CH_3$ spin-system (Fig. 2). The element of the pulse-scheme enclosed in a rectangular box achieves suppression of the central (slowly relaxing; labeled with $R^S_{2,H}$ in Fig. 2) ^{1}H transitions in $^{13}CH_3$ spin-systems and is very similar to that developed by Pervushin and Vögeli [32] for the measurement of ^{1}H–^{1}H residual dipolar couplings in methyl groups of proteins. Briefly, after a polarization state is created at time point '*a*' of the scheme (after the application of gradient g5; Fig. 5a), the ^{1}H transitions of a $^{13}CH_3$ group are excited by the application of a 90°_y pulse, and the $^1J_{CH}$ coupling is allowed to evolve for a time period 2ζ (corresponding to the 'magic angle evolution' delay $2\pi J\zeta = 54.7°$). After application of another 90°_y ^{1}H pulse (time point '*b*'; Fig. 5a), the contribution to the $^{13}CH_3$ signal from ^{1}H transitions of the two $I = 1/2$ manifolds is opposite in sign to the contribution from ^{1}H transitions of the manifold $I = 1$ (Fig. 2), effectively leading to a null in the excitation of the central ^{1}H transitions in a $^{13}CH_3$ group. Subsequently, the outer (fast relaxing; $R^F_{2,H}$ in Fig. 2) ^{1}H transitions of $^{13}CH_3$ methyls are eliminated by the MQ filter between the 90° ^{13}C pulse with phase $\varphi 1$ and time point '*c*' in Fig. 5a [24,33]. The magnetization of $^{13}CHD_2$ methyls evolving during t_1 and t_2 periods of the scheme in Fig. 5a is reduced in the absence of relaxation by a factor of $\sin(2\pi J\zeta)\cos(\pi J\Delta)$ that is equal to 0.58 for the values of the delays used in the experiment of Fig. 5a.

As it is illustrated in Fig. 5b–d, virtually complete suppression of $^{13}CH_3$ signals has been achieved in [3-$^{13}C_1$-pyruvate; 99% D_2O]-derived sample ubiquitin (27 °C) using the scheme of Fig. 5a, with residual $^{13}CH_3$ correlations having intensities lower than those of truncation artifacts of $^{13}CHD_2$ peaks. However, the losses in $^{13}CHD_2$ peak intensities – the fraction of observed $^{13}CHD_2$ intensities relative to $^{13}CHD_2$ intensities in the HSQC spectrum with ^{2}H decoupling varies from 0.52 to 0.60 for the subset of peaks in Fig. 5b – are substantially larger than in the experiment of Fig. 1. Furthermore, the multiple-quantum nature of the former experiment makes it unsuitable for many applications that require the presence of in-phase single-quantum magnetization before the t_1 evolution period. In addition, since the elimination of the central ^{1}H transitions ($R^S_{2,H}$) relies upon the presence of fast-relaxing ^{1}H coherences ($R^F_{2,H}$), the suppression of $^{13}CH_3$ signals by the scheme of Fig. 5a is quite intolerant to fast ^{1}H–^{1}H cross-correlated relaxation within $^{13}CH_3$ methyl groups effective during the delay 2ζ. Therefore, the scheme of Fig. 1 is preferable unless very high levels of $^{13}CH_3$ suppression are desired in samples of small proteins.

Acknowledgments

V.T. thanks the University of Maryland for continuous support. X.L. is on leave from the Department of Chemistry, Xiamen University, China and acknowledges the financial support of the China Scholarship Council (CSC). The authors thank Dr. Chenyun Guo (University of Maryland) for providing the [3-$^{13}C_1$-pyruvate; 99% D_2O]-derived and [U-^{13}C-glucose; 65% D_2O/35% H_2O]-derived samples of human ubiquitin.

References

[1] M.K. Rosen, K.H. Gardner, R.C. Willis, W.E. Parris, T. Pawson, L.E. Kay, Selective methyl group protonation of perdeuterated proteins, J. Mol. Biol. 263 (1996) 627–636.
[2] K.H. Gardner, M.K. Rosen, L.E. Kay, Global folds of highly deuterated, methyl protonated proteins by multidimensional NMR, Biochemistry 36 (1997) 1389–1401.
[3] K.H. Gardner, L.E. Kay, The use of ^{2}H, ^{13}C, ^{15}N multidimensional NMR to study the structure and dynamics of proteins, Annu. Rev. Biophys. Biomol. Struct. 27 (1998) 357–406.
[4] R. Ishima, J.M. Louis, D.A. Torchia, Transverse C-13 relaxation of CHD_2 methyl isotopomers to detect slow conformational changes of protein side chains, J. Am. Chem. Soc. 121 (1999) 11589–11590.
[5] A.L. Lee, P.F. Flynn, A.J. Wand, Comparison of ^{2}H and ^{13}C NMR relaxation techniques for the study of protein methyl group dynamics in solution, J. Am. Chem. Soc. 121 (1999) 2891–2902.
[6] R. Ishima, A.P. Petkova, J.M. Louis, D.A. Torchia, Comparison of methyl rotation axis order parameters derived from model-free analyses of ^{2}H and ^{13}C longitudinal and transverse relaxation rates measured in the same protein sample, J. Am. Chem. Soc. 123 (2001) 6164–6171.
[7] A. Mittermaier, L.E. Kay, Effect of deuteration on some structural parameters of methyl groups in proteins as evaluated by residual dipolar couplings, J. Biomol. NMR 23 (2002) 35–45.
[8] R. Ishima, J.M. Louis, D.A. Torchia, Characterization of two hydrophobic methyl clusters in HIV-1 protease by NMR spin relaxation in solution, J. Mol. Biol. 305 (2001) 515–521.
[9] U. Brath, M. Akke, D. Yang, L.E. Kay, F.A. Mulder, Functional dynamics of human FKBP12 revealed by methyl ^{13}C rotating frame relaxation dispersion NMR spectroscopy, J. Am. Chem. Soc. 128 (2006) 5718–5727.
[10] C. Guo, V. Tugarinov, Selective ^{1}H–^{13}C NMR spectroscopy of methyl groups in residually protonated samples of large proteins, J. Biomol. NMR 46 (2010) 127–133.
[11] R. Otten, B. Chu, K.D. Krewulak, H.J. Vögel, F.A. Mulder, Comprehensive and cost-effective NMR spectroscopy of methyl groups in large proteins, J. Am. Chem. Soc. 132 (2010) 2952–2960.
[12] G. Bodenhausen, J. Ruben, Natural abundance nitrogen-15 NMR by enhanced heteronuclear spectroscopy, Chem. Phys. Lett. 69 (1980) 185–189.
[13] V. Tugarinov, P.M. Hwang, J.E. Ollerenshaw, L.E. Kay, Cross-correlated relaxation enhanced ^{1}H–^{13}C NMR spectroscopy of methyl groups in very high molecular weight proteins and protein complexes, J. Am. Chem. Soc. 125 (2003) 10420–10428.
[14] L.E. Kay, T.E. Bull, L.K. Nicholson, C. Griesinger, H. Schwalbe, A. Bax, D.A. Torchia, The measurement of heteronuclear transverse relaxation times in AX_3 spin systems via polarization transfer techniques, J. Magn. Reson. 100 (1992) 538–558.
[15] L.E. Kay, T.E. Bull, Heteronuclear transverse relaxation in AMX, AX_2, and AX_3 spin systems, J. Magn. Reson. 99 (1992) 615–622.
[16] L.E. Kay, D.A. Torchia, The effects of dipolar cross-correlation on ^{13}C methyl-carbon T_1, T_2 and NOE measurements in macromolecules, J. Magn. Reson. 95 (1991) 536–547.
[17] R. Ishima, J.M. Louis, D.A. Torchia, Optimized labeling of $^{13}CHD_2$ methyl isotopomers in perdeuterated proteins: potential advantages for ^{13}C relaxation studies of methyl dynamics of larger proteins, J. Biomol. NMR 21 (2001) 167–171.
[18] V. Tugarinov, J.E. Ollerenshaw, L.E. Kay, Probing side-chain dynamics in high molecular weight proteins by deuterium NMR spin relaxation: an application to an 82 kDa enzyme, J. Am. Chem. Soc. 127 (2005) 8214–8225.
[19] V. Tugarinov, L.E. Kay, Quantitative ^{13}C and ^{2}H NMR relaxation studies of the 723-residue enzyme malate synthase G reveal a dynamic binding interface, Biochemistry 44 (2005) 15970–15977.
[20] V. Tugarinov, L.E. Kay, Methyl groups as probes of structure and dynamics in NMR studies of high-molecular-weight proteins, Chembiochem 6 (2005) 1567–1577.
[21] T.L. Religa, L.E. Kay, Optimal methyl labeling for studies of supra-molecular systems, J. Biomol. NMR 47 (2010) 163–169.
[22] A.J. Baldwin, T.L. Religa, D.F. Hansen, G. Bouvignies, L.E. Kay, $^{13}CHD_2$ methyl group probes of millisecond time scale exchange in proteins by ^{1}H relaxation dispersion: an application to proteasome gating residue dynamics, J. Am. Chem. Soc. 132 (2010) 10992–10995.
[23] J.E. Ollerenshaw, V. Tugarinov, L.E. Kay, Methyl TROSY: explanation and experimental verification, Magn. Reson. Chem. 41 (2003) 843–852.
[24] D. Sheppard, R. Sprangers, V. Tugarinov, Experimental approaches for NMR studies of sidechain dynamics in high-molecular-weight proteins, Prog. Nucl. Magn. Reson. Spectrosc. 56 (2010) 1–45.
[25] G. Kontaxis, A. Bax, Multiplet component separation for measurement of methyl ^{13}C–^{1}H dipolar couplings in weakly aligned proteins, J. Biomol. NMR 20 (2001) 77–82.
[26] D.M. Doddrell, D.T. Pegg, M.R. Bendall, Distortionless enhancement of NMR signals by polarization transfer, J. Magn. Reson. 48 (1982) 323–327.
[27] G.A. Morris, R. Freeman, Enhancement of nuclear magnetic resonance signals by polarization transfer, J. Am. Chem. Soc. 101 (1979) 760–762.
[28] O.W. Sorensen, R.R. Ernst, Elimination of spectral distortion in polarization transfer experiments. Improvements and comparison of techniques, J. Magn. Reson. 51 (1983) 477–489.

[29] A.G. Palmer, P.E. Wright, M. Rance, Measurement of relaxation time constants for methyl groups by proton-detected heteronuclear NMR spectroscopy, Chem. Phys. Lett. 185 (1991) 41–46.
[30] L.K. Nicholson, L.E. Kay, D.M. Baldisseri, J. Arango, P.E. Young, A. Bax, D.A. Torchia, Dynamics of methyl groups in proteins as studied by proton-detected C-13 NMR-spectroscopy – application to the leucine residues of staphylococcal nuclease, Biochemistry 31 (1992) 5253–5263.
[31] G.W. Vuister, A. Bax, Resolution enhancement and spectral editing of uniformly ^{13}C-enriched proteins by homonuclear broadband ^{13}C decoupling, J. Magn. Reson. 98 (1992) 428–435.
[32] K. Pervushin, B. Vögeli, Observation of individual transitions in magnetically equivalent spin systems, J. Am. Chem. Soc. 125 (2003) 9566–9767.
[33] D.M. Korzhnev, K. Kloiber, V. Kanelis, V. Tugarinov, L.E. Kay, Probing slow dynamics in high molecular weight proteins by methyl-TROSY NMR spectroscopy: application to a 723-residue enzyme, J. Am. Chem. Soc. 126 (2004) 3964–3973.
[34] A.J. Shaka, J. Keeler, T. Frenkiel, R. Freeman, An improved sequence for broadband decoupling: WALTZ-16, J. Magn. Reson. 52 (1983) 335–338.
[35] D. Marion, M. Ikura, R. Tschudin, A. Bax, Rapid recording of 2D NMR spectra without phase cycling. Application to the study of hydrogen exchange in proteins, J. Magn. Reson. 85 (1989) 393–399.